Journal of Applied Electrochemistry (2022) 52:1295–1304
https://doi.org/10.1007/s10800-022-01712-y

RESEARCH ARTICLE

Two-dimensional Fe-TPPHZ nanosheets for electrohydrogenation of N_2 to NH_3 under ambient conditions

Ying Wang[1] · Hui Luo[1] · Chaoxu Ye[1] · Yanjun Shi[1] · Zhidong Chen[1] · Wenchang Wang[1] · Jianyu Cao[1] · Juan Xu[1]

Received: 10 November 2021 / Accepted: 2 May 2022 / Published online: 21 May 2022

Abstract

The design of high-performance and low-cost catalysts for mild electrocatalytic nitrogen reduction reaction (NRR) is particularly desirable and remains greatly challenging due to the unfavorably low ammonia yield rate and Faradaic efficiency (FE), which comes from the difficulty in making nitrogen activation superior to competitive hydrogen evolution reaction (HER). Herein, we report a well-designed two-dimensional nanosheet-like Fe-tetrapyridophenazine (Fe-TPPHZ) catalyst for ambient NRR process, which was facially prepared by coordinating Fe ions with TPPHZ ligand. The Fe-TPPHZ catalyst shows a remarkable NRR activity at ambient conditions with a high NH_3 yield rate of 29.07 μg h^{-1} mg^{-1} and an outstanding FE of 11.5% at − 0.3 V vs. RHE. An ammonia yield rate of 21.86 μg h^{-1} mg^{-1} is observed after 100 consecutive cycles, with a retention rate of 75.2%. This work will provide a rational design idea to use non-precious metal-based complex as highly effective electrocatalysts for NRR test.

Graphical Abstract

A two-dimensional nanosheet-like Fe-tetrapyridophenazine (Fe-TPPHZ) catalyst was successfully designed and utilized for ambient NRR process, showing a remarkable NRR activity with a high NH_3 yield rate of 29.07 μg h^{-1} mg^{-1}, outstanding FE of 11.5% at − 0.3 V vs. RHE and good retention rate of 75.2% after 100 cycles.

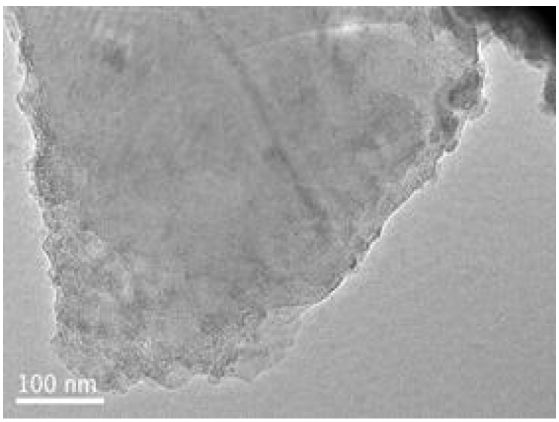

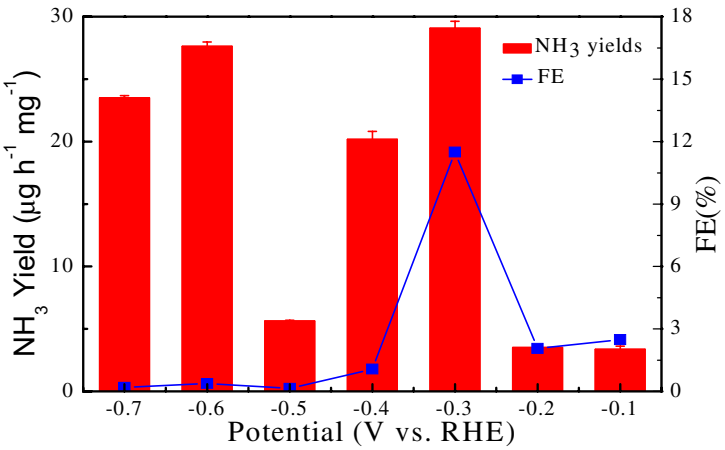

Keywords Nitrogen reduction reaction · Fe-tetrapyridophenazine · Ammonia yield rate

1 Introduction

Ammonia plays an important role in human life and industrial production because of its wide application in fiber, chemical fertilizer, pharmaceutical, energy storage

✉ Jianyu Cao
jycao@cczu.edu.cn

✉ Juan Xu
cjytion@cczu.edu.cn

Extended author information available on the last page of the article

intermediate and other fields [1]. Nowadays, available ammonia preparation methods can be classified into industrial Haber-Bosch, natural biological, plasma discharge, photocatalytic and electrochemical nitrogen fixation process. Although the traditional Haber-Bosch reduction process has dominated the industrial scale NH_3 synthesis field, it usually suffers from low efficiency, high fossil energy consumption and severe operation conditions (ca. 700 K and ca. 100 atm) even with some optimized catalysts due to the stable triple bond of nitrogen molecules (945 kJ mol^{-1}), low polarization level and high ionization energy [2, 3]. Therefore, it remains a great challenge to look for effective methods to promote the industrial scale ammonia production via effectively adsorbing and activating nitrogen [4, 5]. Meanwhile, biological nitrogen fixation cannot meet human needs for NH_3 development due to its low yield, uncontrollable reaction process and slow reaction rate [6]. Comparatively speaking, photocatalytic and electrochemical nitrogen fixation are two sustainable and green methods for ammonia synthesis due to their ambient working conditions and low energy consumption mode, and the electrochemical nitrogen fixation process shows a higher ammonia yield, easier handling conditions and wider application field [7].

The biggest challenge of electrochemical ammonia synthesis lies in the search and design of highly effective electrocatalysts to activate the ultra-highly stable three bonds of nitrogen molecules, promote N_2 reduction reaction (NRR) kinetics and weaken hydrogen evolution reaction (HER) interference. As a suitable catalyst for NRR, it should satisfy four prerequisites: high ammonia yield rate, satisfactory faraday efficiency, excellent activity and good selectivity. In general, various design strategies for the reported catalysts can be classified into four categories, that is, defect engineering, structural manipulation, crystallographic tailoring, and interface regulation [6]. So far, a series of effective catalysts have been prepared to electrochemically reduce nitrogen to ammonia, which contain precious metals (e.g., Ru [8], Rh [9], Au [10] and Pt [11], etc.), non-precious metals compounds (e.g., Fe [12], foam nickel [13], MoS_2 [14], VN [15], etc.) and metal-free nanomaterials (e.g. C_3N_4 [16], B-doped graphene [17], N-doped carbon [18], B_4C [19], black phosphorus nanosheets [20], etc.). Among these effective catalysts, non-precious metal Fe-based nanomaterials presented a promising catalytical effect on the electrochemical nitrogen reduction, which exhibited an outstanding activity and feasibility for electrocatalytic NRR [21–24]. For example, inspired by the role of biological nitrogenase, FeMo nanoclusters/single atoms was designed and synthesized on porous nitrogen-doped carbon (FeMo/NC) [25], indicating a stable Faradaic efficiency (FE) (ca. 11.8%) at -0.25 V and NH_3 yield rate (ca. 26.5 $\mu g h^{-1} mg^{-1}{}_{cat}$.) at -0.3 V in neutral electrolyte. Moreover, the appearance of the single-atom Fe on nitrogen-doped carbon can achieve a maximum Faradaic efficiency of 56.55% and special positive initial potential of 0.193 V for NH_3 production [26]. The single Fe atoms supported on nitrogen-doped carbon can bring a FE of 8.4% at -0.2 V [27]. As reported [24], the optimized charge transfer between adjacent O and Fe atoms can both promote the electroreduction kinetics of N_2 to NH_3, and effectively reduce the binding energy between atomic Fe catalyst and electrochemical reaction intermediates of N_2. Wang et al. found the porous Fe_2O_3 nanorods supported on carbon cloth provided a high NH_3 yield of 6.78 $\mu g h^{-1} cm^{-2}$ and Faradaic efficiency of 7.69% at -0.4 V [28]. The NH_3 yield that catalyzed by the optimized Fe doped CuS QDs reached to 26.4 $\mu g h^{-1} mg^{-1}{}_{cat}$ at -0.7 V, which quintuples that of the pristine CuS QDs [29]. As proved, nitrogen can be easily captured at ambient temperature by the Fe atoms that incorporated into the graphene layer, exhibiting a special six-proton and six-electron process [30]. More importantly, benefiting from the empty d orbitals of transition metals atoms, Fe-based catalysts can synergistically accept electrons from nitrogen gas molecules with appropriate electronic energy and symmetry [31]. At the same time, metal Fe atoms act as electron acceptors to donate electrons to the π^* orbitals of nitrogen molecules, strengthening their adsorption and activating the triple bonds of nitrogen molecules [32]. Most of these Fe-based catalysts are porous carbon supported single-atom Fe catalyst, and their stability and practical application prospect are questionable. In this work, one novel Fe-based complex catalyst, Fe-tetrapyridophenazine (Fe-TPPHZ) was synthesized and utilized to electrochemically catalyze nitrogen. The TPPHZ can be used as one ideal protective agent for metal catalysts, which can restrain them from aggregating and deactivating. Furthermore, the nitrogen atoms of the TPPHZ help to boost the ambient nitrogen reduction reactions [33].

2 Experimental section

2.1 Chemicals and reagents

All chemicals were used as obtained without further purification. Tetrapyridophenazine (TPPHZ, 98 wt%) was purchased from Jinan Henghua Technology Co., Ltd. (China). N-N-dimethylformamide (DMF, 99.5%), dichloromethane, isopropanol, ethanol, ferrous sulfate heptahydrate, potassium hydroxide, sodium hydroxide, sulfuric acid, hydrochloric acid, sodium salicylate, potassium sodium tartrate, sodium hypochlorite, ammonium chloride, p-Dimethylaminobenzaldehyde, hydrazine hydrochloride and sodium nitroprusside (99.0 wt%) were bought from Sinopharm Chemical Reagent Co., Ltd. (China). Keqin black (KB) comes from Suzhou Yilongsheng Energy Technology Co., Ltd (China). Nafion solution (5 wt%) was provided by Nation DuPont Co., Ltd. (USA).

2.2 Synthesis of Fe-TPPHZ

Fe-TPPHZ was synthesized via a hydrothermal method [34]. Firstly, 0.104 g (0.25 mmol) TPPHZ was put into a 70 mL DMF solution and jointly ultrasonicated for 10 min to form a uniform solution. Secondly, 0.07 g (0.25 mmol) $FeSO_4{\cdot}7H_2O$ was added into the above mixture under vigorous stirring and then they were transferred to a 100 mL Teflon lined stainless steel autoclave together. After being hydrothermally heated at 160 ℃ for 12 h, the sample was handled by a series of centrifugation and washing procedures. In the rinse process, the unreacted TPPHZ was washed off with dichloromethane. Finally, the brown solid product was dried in vacuum oven at 60 ℃ overnight and collected.

2.3 Physical characterization

X-Ray Diffraction (XRD) test was determined by a D/max-2000 XRD diffractometer (Cu target, $\lambda = 1.50456$ Å) from Rigaku Co., Japan. Scanning electron microscope (SEM) measurement was made by supra 55 sapphire FE-SEM of Carl Zeiss, Germany. Transmission electron microscope (TEM) determination was conducted with JEOL's JEM-2100 F. Brunner-Emmet-Teller (BET) data were obtained by measuring N_2 adsorption-disadsorption isotherms at 77 K using Micromeritics ASAP 2020 analyzer. X-ray photoelectron spectroscopy (XPS) spectra were characterized with a thermo escalab 250 energy spectrometer and analyzed with XPSPEAK software. Ultraviolet–visible (UV–Vis) test was conducted with a mini-1240 UV spectrophotometer of Shimadzu Corporation of Japan.

2.4 Electrochemical measurements

2.4.1 Pretreatment of carbon paper and nafion 117 membrane

As the substrate of cathode, carbon paper was ultrasonicated for 10 min in isopropanol solution, and then immersed in concentrated sulfuric acid and hydrogen peroxide solution, respectively, for 5 h at 50 ℃. Finally, it was washed with deionized water to neutral, and then kept in deionized water.

In the case of the Nafion 117 membrane, it was put into the pre-prepared H_2O_2 solution (5 vol%) and heated in a water bath at 85 ℃ for 2 h. After being cooled to room temperature, it was boiled in deionized water at 55 ℃ for 30 min, and then boiled in 0.5 M sulfuric acid solution for 2 h at 85 ℃. Finally, the boiled Nafion 117 membrane was washed to neutral and stored in deionized water.

2.4.2 Cathode preparation process

2 mg Fe-TPPHZ, 2 mg Keqin black, 0.5 mL isopropanol and 0.5 mL deionized water were mixed together and ultrasonicated for 30 min. Subsequently, 75 μL Nafion solution (5 wt%) was further added and ultrasonicated for 1 h. Finally, the above uniformly dispersed ink was dropped on the pretreated carbon paper (1 cm^2) or the rotating disk electrode (RDE, 0.1963 cm^2), respectively.

2.4.3 NRR potential selection

Linear sweep voltammetry (LSV) experiments were conducted in Ar- or N_2-saturated 0.1 M KOH solution at room temperature with a rotating disk electrode. The LSV curve was obtained at a scanning rate of 5 mV s^{-1} with a speed of 1,600 rpm. All applied potentials were converted to the reversible hydrogen electrode (RHE) scale via the following calibration equation: $E(\text{vs. RHE}) = E(\text{vs. Hg/HgO}) + 0.059*\text{PH} + 0.098$ [35, 36]. Based on the difference in current densities determined in Ar- or N_2-saturated electrolytes, the potentials that used for the NRR test reaction was selected.

2.4.4 NRR test

Electrohydrogenation of N_2 to NH_3 using Fe-TPPHZ as catalyst was made with a three-electrode system in a typical H-type two-compartment cell. In the whole NRR test process, the above pretreated Nafion 117 membrane was completely immersed to separate cathode and anode chamber.

In the assigned three-electrode system, the Fe-TPPHZ coated carbon paper, platinum sheet and saturated KOH filled Hg/HgO electrode act as the working, counter and reference electrodes, respectively. The chronoamperometry experiments at various measured potentials were conducted with 45 mL 0.1 M KOH as electrolytes in both anode and cathode chamber. N_2 bubbles were filled into the KOH electrolytes for 30 min at the outset of the experiment, and then were continuously purged during NRR measurements. Moreover, magnetic stirring was performed at a rate of 600 rpm throughout the measurements, and a continuous acid trap with 5 mL 0.05 M H_2SO_4 was connected with the cathode chamber. All electrochemical measurements were carried out using a CHI 660E electrochemical analyzer (CH instrument, China) and the applied potentials were calibrated to be that versus RHE.

2.4.5 Quantitative detection of ammonia

Ammonia concentration was quantitatively determined via the generally acknowledged indophenol blue method using the UV–Vis spectrophotometry [22]. Firstly, standard NH_4Cl

solution was utilized to draw the calibration curve of ammonia concentration and absorbance. The calibration process was conducted independently for three times. In brief, pre-dried NH_4Cl was dissolved in 0.1 M KOH and diluted to different concentrations. Then, 2 mL NH_4Cl solution with desired concentration was sequentially added with 2 mL of 1 M NaOH solution containing 5 wt% sodium salicylate and 5 wt% seignette salt as a colour-producing reagent, 1 mL of 0.05 M iodine pre-calibrated NaClO as an oxidation solution and 0.2 mL of 1 wt% sodium nitroferricyanide as a catalytic reagent. After 1 h oxidation reaction at room temperature, the absorption spectrum of the above solution was measured using UV–Vis spectrophotometer. Based on the relationship of ammonia concentration and absorbance at 654 nm, a fitting curve was obtained, showing a reliable and accurate linear relation ($y = 0.336x + 0.172$, $R^2 = 0.999$) (Figure S1). After the electrocatalytic nitrogen reduction reaction, the electrolyte was carefully taken out from the cathodic chamber and added with the same colour-producing, oxidation and catalytic reagent as the above NH_4Cl solution. In the light of the UV–Vis absorbance at 654 nm, the NH_3 concentration in the cathode chamber can be calculated.

In order to determine the NH_3 concentration in the acid trap that was connected with the cathode chamber, a similar calibration curve in the 0.1 M H_2SO_4 media was carried out, which presents a good linear relationship ($y = 0.3624x + 0.0554$, $R^2 = 0.999$) (Figure S2).

2.4.6 Hydrazine (N_2H_4) detection

The production of N_2H_4 was assayed using the reported Watt and Chrisp method [37]. Specially, 5.99 g $C_9H_{11}NO$, 30 mL concentrated HCl and 300 mL C_2H_5OH were mixed together under magnetic stirring and utilized as the color reagent. Then, a series of 5 mL hydrazine dihydrochloride solutions of known concentrations were separately mixed with 5 mL of the above color reagent under magnetic stirring for 20 min at 25 ℃. Subsequently, the calibration curve was acquired by measuring their UV–Vis absorbance at 455 nm, and the linear relation can be displayed as $y = 1.061x + 0.011$ with a good linear correlation ($R^2 = 0.999$) (Figure S3). After the electrochemical reduction process, 5 mL electrolyte was added into 5 mL color reagent, and then detected with the same procedure. The amount of N_2H_4 can be ascertained according to the pre-measured calibration curve of the hydrazine dihydrochloride.

2.4.7 Calculation of NH_3 yield and faraday efficiency (FE)

The NH_3 yield was the sum of produced NH_3 in the cathode chamber, anode chamber and acid trap, which was calculated according to the following equation [38]:

$$\text{Yield}_{(NH3)} = (c \times V)/(t \times m) \quad (1)$$

where c, V, t and m represents the determined NH_3 concentration, volume of electrolyte or acid trap, NRR test time and mass of the Fe-TPPHZ catalyst, respectively.

The FE was calculated based on the following equation and the assumption that three electrons were needed to produce one NH_3 molecule [38]:

$$\text{FE} = 3F \times c \times V / (M \times Q)$$

where F, c, V, M and Q stands for the Faraday constant, NH_3 concentration, volume of electrolyte or acid trap, molecular weight of NH_3 and charge quantity at diverse applied potential that comes from the integral of I–t curves.

3 Results and discussions

3.1 Physical characterization

The composition and surface chemical state were investigated by XPS. Figure 1 shows the XPS survey spectrum of Fe-TPPHZ and the corresponding fitted deconvolutions of Fe 2p, N 1s and C 1s. As illustrated, the peaks centered at ca. 283, 399, 530 and 710.08 eV can be ascribed to the Fe, C, N and O elements, respectively (Fig. 1a). For the fitted high-resolution spectra of Fe 2p, the peaks situated at 710 eV (Fe $2p_{3/2}$) and 723.3 eV (Fe $2p_{1/2}$) can be assigned to Fe^{2+}, and the peaks at 713.1 eV (Fe $2p_{3/2}$) and 725.2 eV(Fe $2p_{1/2}$) belongs to Fe^{3+}(Fig. 1b). Moreover, the peak integral area ratio of the Fe^{2+} and Fe^{3+} in Fe-TPPHZ is 1:1, indicating that the percentage of Fe^{2+} and Fe^{3+} is almost the same. The N 1s spectrum shows two peaks at 398.5 and 399.1 eV (Fig. 1c), which is the typical signal of pyridine nitrogen and pyrrole nitrogen. The fine spectrum of C 1s shows that the binding energy peaks located at 284.7, 285.6 and 288 eV are attributed to C–C, C–N and C=O functional groups, respectively (Fig. 1d). The existence of the pyridine and pyrrole nitrogen atoms can realize the strong adsorption of nitrogen molecules and the easy dissociation of their triple bonds [39], introducing important synergistic electrocatalytic performances on the interface [40]. Furthermore, carbon atoms derived from the conjugated TPPHZ molecular contributes to the elevation of electronic conductivity of catalysts.

The morphology and nanostructure of the as-synthesized Fe-TPPHZ was identified by SEM and TEM. Figure 2 shows the SEM and TEM images of the Fe-TPPHZ. As seen from the images, the Fe-TPPHZ presents an aggregated two-dimensional nanosheet structure (Fig. 2c) and their thickness is less than 5 nm (Fig. 2d). In addition, several thin nanosheets stacked together and formed smooth surfaces and rough edges, which helps to enhance the catalytical effect on

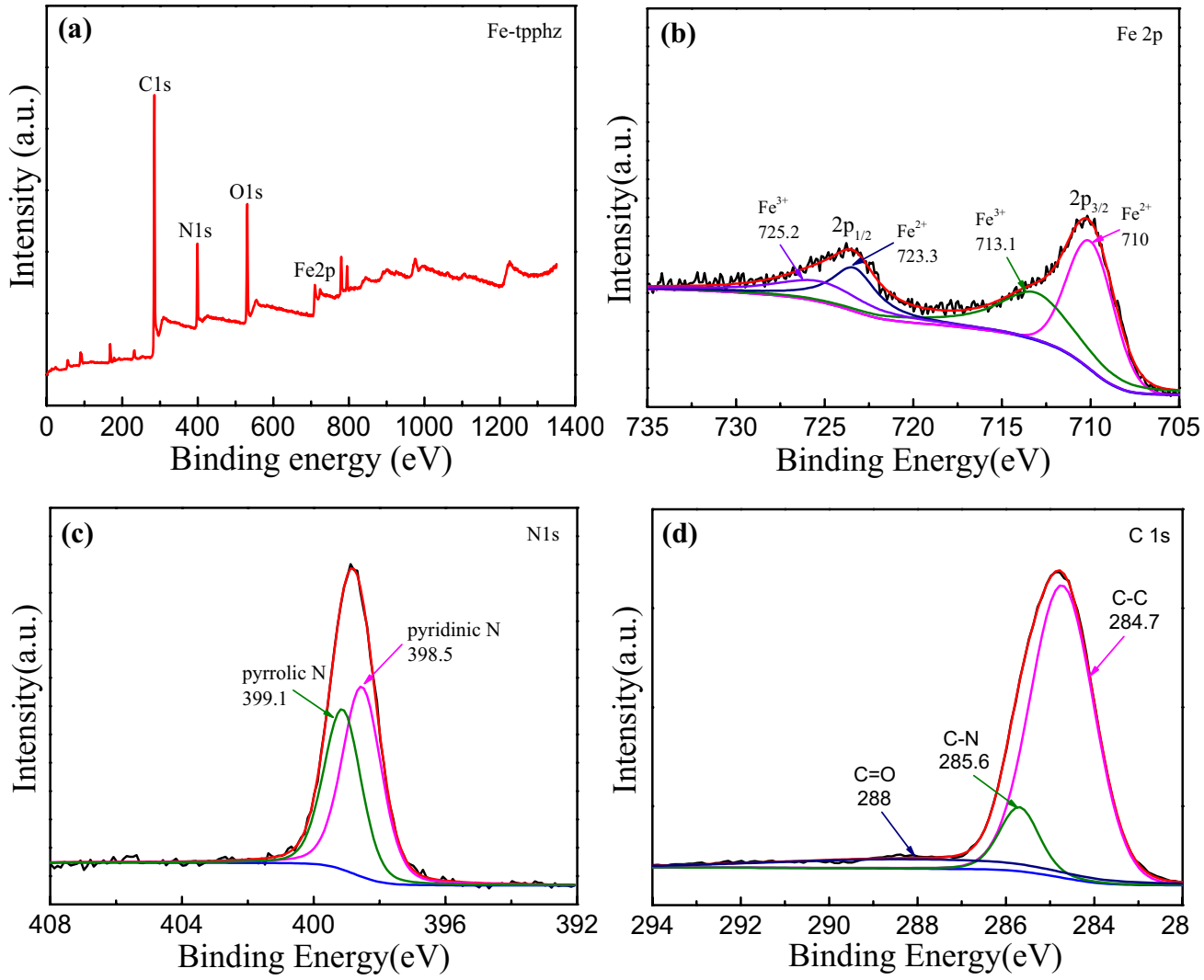

Fig. 1 XPS survey spectrum of Fe-TPPHZ (**a**) and the corresponding fitted deconvolutions of Fe 2p (**b**), N 1s (**c**) and C 1s (**d**)

NRR because that the sheet-like morphology can bring an extended specific surface area and affluent catalytic active sites [41].

The crystallinity structure of the samples was analyzed by X-ray diffraction meter. Figure 3 presents XRD patterns of the TPPHZ and as-prepared Fe-TPPHZ. As illustrated, the TPPHZ shows the characterized peak at 10.3°, 26°, 29.1 °, 39.4 ° and 43.1 °. After being conjugated with Fe ions, the peak location of the TPPHZ almost remains the same, but their relative peak intensity changed. Furthermore, new peaks at 11.5, 33.2° and 50.3° appeared, indicating the successful formation of Fe-TPPHZ molecules.

Figure 4 displays the BET data of the as-prepared Fe-TPPHZ. The corresponding value is shown in Table 1. The values of the specific area, pore volume and average pore size are 268. 6 $m^2\ g^{-1}$, 0.436 $cm^3\ g^{-1}$ and 5.3 nm. This high specific area and nanoporous structure help to provide more active sites to adsorb and catalyze nitrogen reduction reaction.

3.2 NRR performances

As proved in literature [42], K^+ ion in the electrolyte can closely interrelate with nitrogen molecules, promote their stern layer interlacement, and enhance the aggregation of nitrogen on the surface of catalysts. Meanwhile, alkaline electrolytes are more effective to weaken the interference of HER than acidic medium [11]. Thus, 0.1 M KOH (pH 13) was selected as the electrolyte for all NRR determination. The whole NRR measurement process was carried out at various applied potential in a conventional H-type electrochemical cell with either N_2 or Ar bubbled KOH electrolyte on an electrochemical workstation (CHI 660E) at room temperature. In the three-electrode system, the working

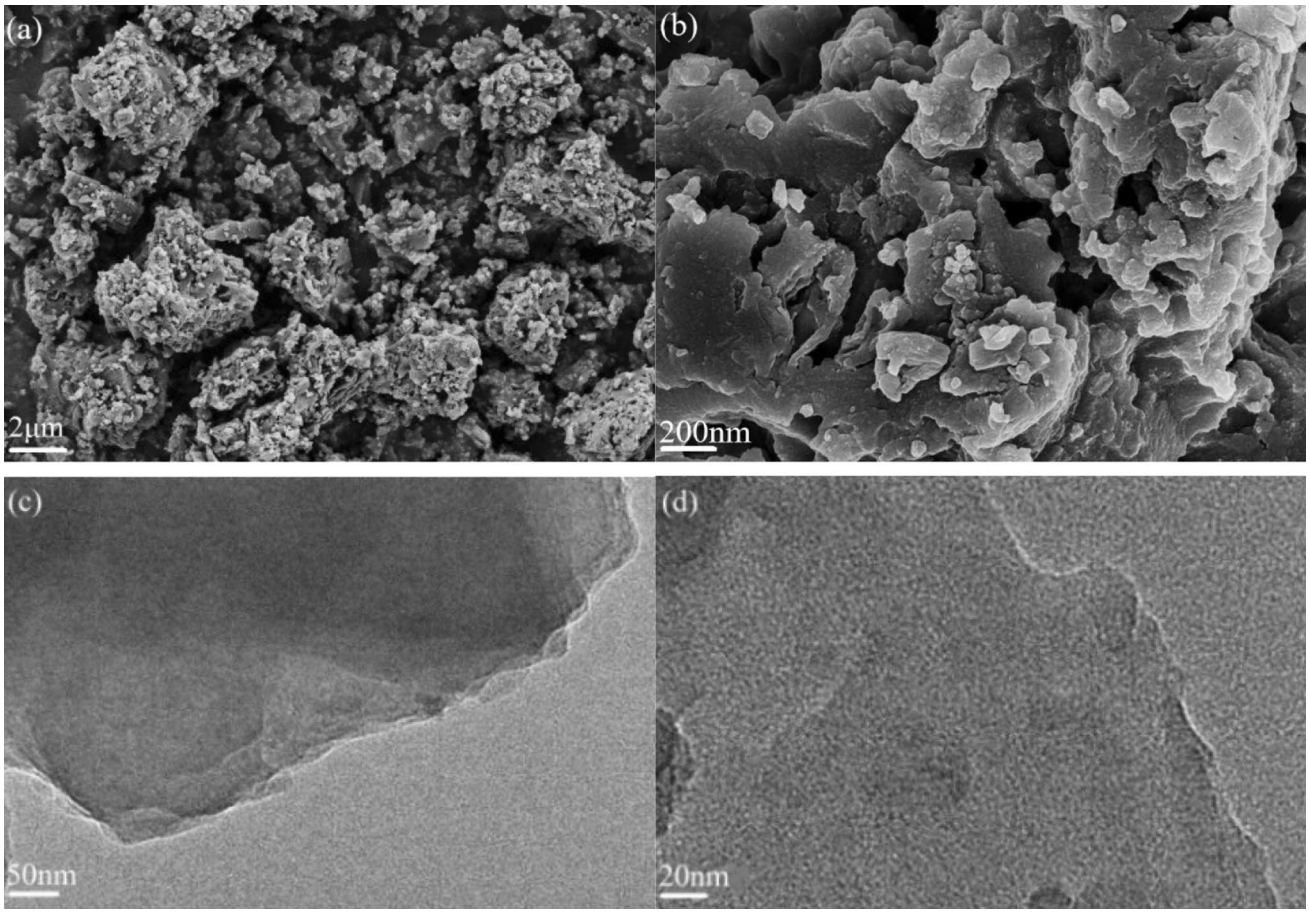

Fig. 2 SEM (**a**, **b**) and TEM (**c**) pictures of the as-prepared Fe-TPPHZ

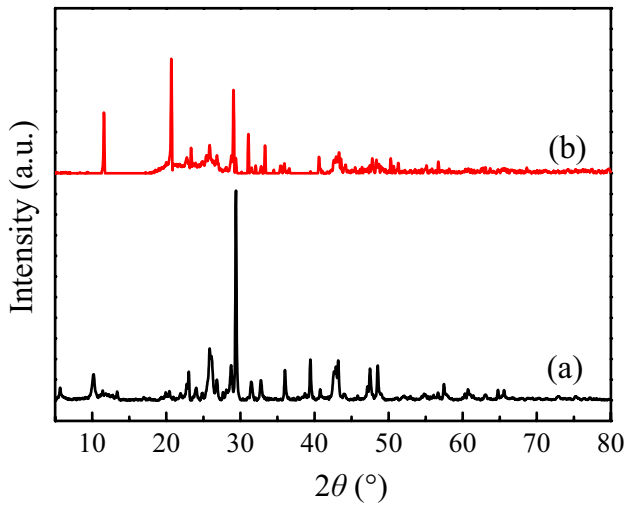

Fig. 3 XRD patterns of the TPPHZ (**a**) and as-prepared Fe-TPPHZ (**b**)

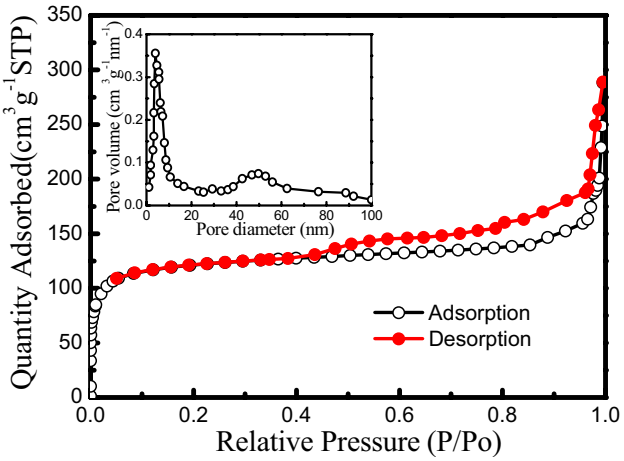

Fig. 4 BET data of the as-prepared Fe-TPPHZ

and reference electrodes were put in the cathode area, and the counter electrode was separated in the anode area by a Nafion 117 membrane. The continually purged nitrogen in KOH electrolyte around the cathode obtained electrons to

Table 1 BET Parameters of the as-prepared Fe-TPPHZ

Sample	Specific area (m^2g^{-1})	Pore volume (cm^3g^{-1})	Average pore size(nm)
Fe-TPPHZ	268. 6	0.436	5.3

generate ammonia, and the hydroxyl ions around the anode converted to oxygen and water by losing electrons. In order to eliminate the possible interferences of ammonia or oxynitride in the inputted N_2 or Ar gases, they were pre-purified via a series of devices with 0.1 M NaOH, 0.1 M $FeSO_4$ and 5 mM H_2SO_4 solutions.

Linear sweep voltammograms (LSV) curves were determined to preliminarily evaluate the electroreduction effect of the as-prepared Fe-TPPHZ catalyst on the NRR test. Figure 5 presents the LSV curves of the Fe-TPPHZ in Ar- or N_2-saturated KOH electrolyte. The reduction current increase in the Ar-saturated KOH solution comes from the competing HER, which was used to break the strong H–O–H covalent bonds before hydrogen adsorption. An obvious increase in the reduction current density between −0.3 to −0.7 V (vs. RHE) was observed in the N_2-saturated electrolyte than in the Ar-saturated one, suggesting a high catalytic effect of Fe-TPPHZ on the reduction of nitrogen in this region.

The NRR performances of the Fe-TPPHZ were then elaborately investigated in a three-electrode system using 0.1 M KOH as electrolyte at various potentials with incessant N_2 bubbling in the cathode chamber. All the NRR experiments were performed at room temperature. Meanwhile, a glass tube with diluted H_2SO_4 was placed at the end of the cell as acid trap to fully adsorb escaped NH_3 that was caused by N_2 blowing. The total NH_3 yield was the sum of produced ammonia in the cathode chamber, anode chamber and acid trap, which was quantitatively examined by the universally acknowledged indophenol blue method. The UV-Vis absorption curves of the electrolytes after the NRR tests are illustrated at different given potentials (Figure S4). Figure 6 presented the average mass-normalized NH_3 yield rates and corresponding Faradaic efficiencies of the Fe-TPPHZ at different potentials. As illustrated, the highest NH_3 yield rate of 29.07 μg h^{-1} mg^{-1} was achieved with an outstanding Faradaic efficiency of 11.5% at -0.3 V vs. RHE. With the negative shift of the given potential from −0.3 to −0.7 V, the Faradaic efficiency gradually decreases due to the competing reaction of the HER.

In the NRR process, hydrazine (N_2H_4) was considered as the possible by-product and the systematically detected spectrophotometric results showed that no hydrazine was generated in the Fe-TPPHZ catalyzed system (Figure S5).

Figure 7 displays the mass-normalized NH_3 yield rates and corresponding Faradaic efficiencies of the Fe-TPPHZ,

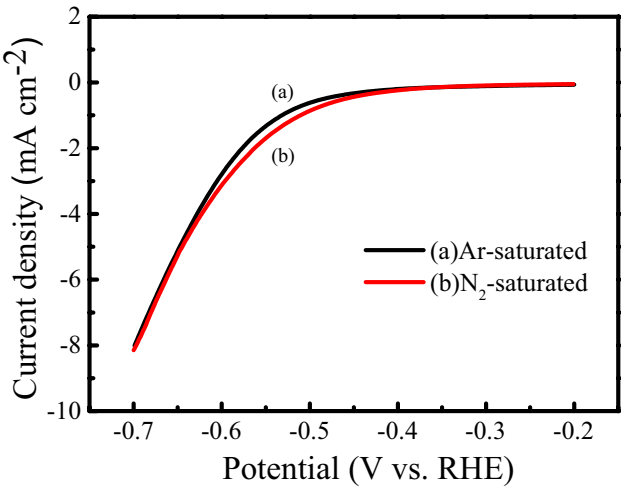

Fig. 5 Linear sweep voltammograms of Fe-TPPHZ in Ar- (black line) or N_2-saturated (red line) 0.1 M KOH solution at a scan rate of 5 mV s^{-1}

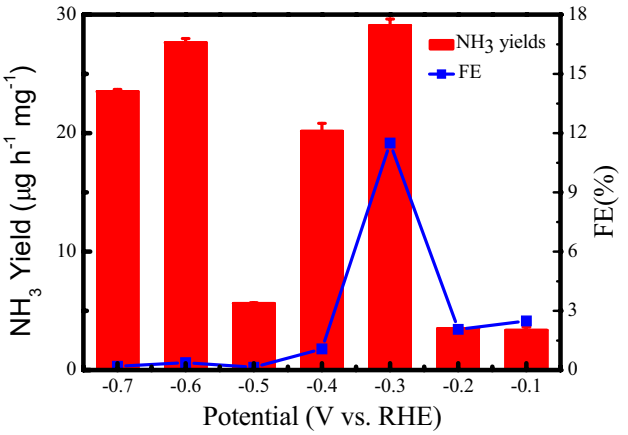

Fig. 6 The mass-normalized NH_3 yield rates (left y axis) and corresponding Faradaic efficiencies (right y axis) of the Fe-TPPHZ at different applied potentials. The error bars show the average value of three measurements

pristine Fe and TPPHZ at -0.3 V versus RHE. In the case of the pristine Fe, the NH_3 yield rate and Faradaic efficiency at -0.3 V is only 9.77 μg h^{-1} mg^{-1} and 0.71%, and the values for the TPPHZ are 5.1 μg h^{-1} mg^{-1} and 2.6%, which demonstrated that the Fe-TPPHZ possesses catalytic superiority than Fe and TPPHZ. It can be predicted that the greatly improved NRR performances of the Fe-TPPHZ may originate from the isolating role of the TPPHZ molecular on active Fe sites, which can utilize their conjugated aromatic ring to ensure the independence and homogeneity of the Fe active sites in the course of NRR test [34].

To further assess the catalytical performances of the Fe-TPPHZ, the mass-normalized NH_3 yield rate of the Fe-TPPHZ was compared with literature values, as shown

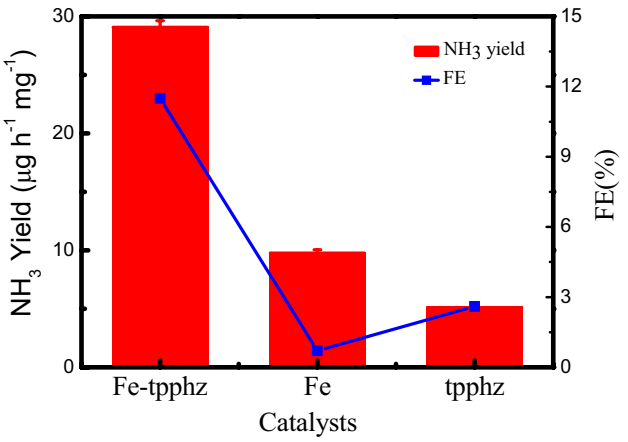

Fig. 7 The mass-normalized NH_3 yield rates and corresponding Faradaic efficiencies of Fe-TPPHZ, pristine Fe and TPPHZ at −0.3 V versus RHE in 0.1 M KOH

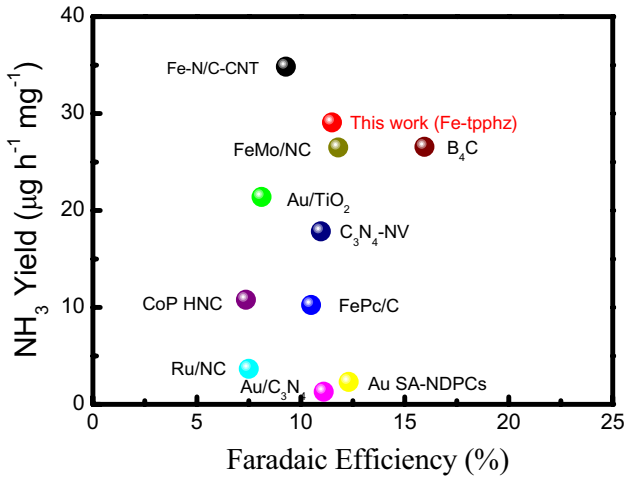

Fig. 8 Comparison of the mass-normalized NH_3 yield rates of the Fe-TPPHZ with literature values

in Fig. 8. Clearly, the as-prepared Fe-TPPHZ attained a higher NH_3 yield rate than most reported catalysts.

Figure 9 shows the chronoamperometric curves at different applied potentials and the NRR stability test of Fe-TPPHZ at −0 to −0.3 V versus RHE. The insets show the chronoamperometry test of the Fe-TPPHZ at −0.3 V for 12 h and the FE change after 8 cycles. Almost no current density change was detected for the Fe-TPPHZ at −0.3 V during the initial 2 h test and only a small fluctuation in current density was found after the long-time chronoamperometric measurement (Fig. 9A). An ammonia yield rate of 21.86 μg h^{-1} mg^{-1} is observed after 100 consecutive cycles with a retention rate of 75.2% (Fig. 9B), indicating a good stability.

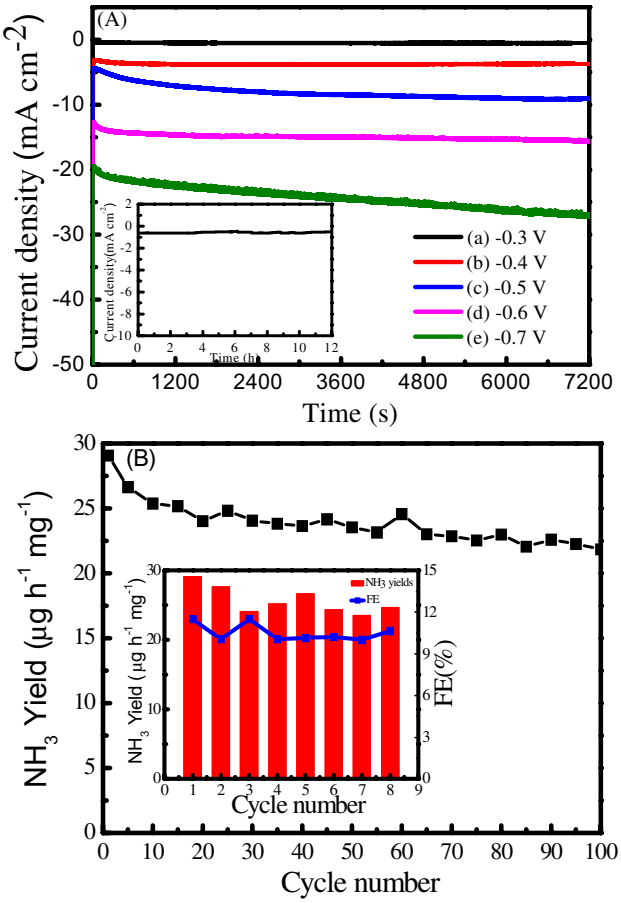

Fig. 9 **A** Chronoamperometric curves at different applied potentials and **B** NRR stability test of Fe-TPPHZ at −0.3 V versus RHE. The insets show the chronoamperometry test of the Fe-TPPHZ at −0.3 V for 12 h and the FE change after 8 cycles

4 Conclusions

Novel Fe-TPPHZ nanosheets were synthesized via a hydrothermal way and utilized as highly effective catalysts for the electrocatalytic nitrogen reduction under mild conditions. The as-prepared Fe-TPPHZ nanosheets displayed a remarkable catalytic performance, with a high NH_3 yield of 29.07 μg h^{-1} mg^{-1} and an outstanding Faradaic efficiency of 11.5% at −0.3 V vs. RHE. Meanwhile, no hydrazine appearance and NH_3 yield change was found during the NRR process for 2 h at −0.3 V vs. RHE, demonstrating a good selectivity and stability. This work developed a new catalyst for electrochemical production of NH_3 from N_2.

Supplementary Information The online version contains supplementary material available at https://doi.org/10.1007/s10800-022-01712-y.

Acknowledgements This work was financially supported by the National Natural Science Foundation of China (21773018 and 21975033) and the Analysis and Testing Center, NERC Biomass of Changzhou University.

References

1. Liu Q, Xu T, Luo Y, Kong Q, Li T, Lu S, Alshehri AA, Alzahrani KA, Sun X (2021) Recent advances in strategies for highly selective electrocatalytic N_2 reduction toward ambient NH_3 synthesis. Curr Opin Electrochem 29:100766–100772
2. Tang C, Qiao S-Z (2019) How to explore ambient electrocatalytic nitrogen reduction reliably and insightfully. Chem Soc Rev 48:3166–3180
3. Duan G, Chen Y, Tang Y, Gasem KAM, Wan Ding PD, Fan M (2020) Advances in electrocatalytic ammonia synthesis under mild conditions. Prog Energ Combust 81:100860–100889
4. Xu T, Liang J, Li S, Xu Z, Yue L, Li T, Luo Y, Liu Q, Shi X, Asiri A, Yang M, Sun C X (2021) Recent advances in non-precious metal oxides electrocatalysts and photocatalysts for N_2 reduction reaction under ambient condition. Small Sci 1:2000069–2000086
5. Zhu X, Mou S, Peng Q, Liu Q, Luo Y, Chen G, Gao S, Sun X (2020) Aqueous electrocatalytic N_2 reduction for ambient NH_3 synthesis: recent advances in catalysts developing and performances boosting. J Mater Chem A 8:1545–1556
6. Shi L, Yin Y, Wang S, Sun H (2020) Rational catalyst design for N_2 reduction under ambient conditions: strategies toward enhanced conversion efficiency. ACS Catal 10:6870–6899
7. Cui X, Tang C, Zhang Q (2018) A review of electrocatalytic reduction of dinitrogen to ammonia under ambient conditions. Adv Energy Mater 8:1800369–1800393
8. Kordali V, Kyriacou G, Lambrou C (2000) Electrochemical synthesis of ammonia at atmospheric pressure and low temperature in a solid polymer electrolyte cell. Chem Commun 17:1673–1674
9. Kugler K, Luhn M, Schramm JA, Rahimib K, Wessling M (2015) Galvanic deposition of Rh and Ru on randomly structured Ti felts for the electrochemical NH_3 synthesis. Phys Chem It Phys 17:3768–3782
10. Zhang J, Zhao B, Liang W, Zhou G, Liang Z, Wang Y, Qu J, Sun Y, Jiang L (2020) Three-phase electrolysis by gold nanoparticle on hydrophobic interface for enhanced electrochemical nitrogen reduction reaction. Adv Sci 7:20022630–20022636
11. Lv J, Tian Z, Dai K, Ye Y, Liang C (2019) Interface and defect engineer of titanium dioxide supported palladium or platinum for tuning the activity and selectivity of electrocatalytic nitrogen reduction reaction. J Colloid Interf Sci 553:126–135
12. Hu L, Khaniya A, Wang J, Chen G, Kaden WE, Feng X (2018) Ambient electrochemical ammonia synthesis with high selectivity on Fe/Fe oxide catalyst. ACS Catal 8:9312–9319
13. Li G, Pan Z, Lin H, An L (2021) In-situ formation of bismuth nanoparticles on nickel foam for ambient ammonia synthesis via electrocatalytic nitrogen reduction. J Alloy Compd 875:160006–160013
14. Zhang L, Ji X, Ren X, Ma Y, Shi X, Tian Z, Asiri AM, Chen L, Tang B, Sun X (2018) Electrochemical ammonia synthesis via nitrogen reduction reaction on a MoS_2 catalyst: theoretical and experimental studies. Adv Mater 30:1800191–1800196
15. Yang X, Nash J, Anibal J, Dunwell M, Kattel S, Stavitski E, Attenkofer K, Chen J, Yan Y, Xu B (2018) Mechanistic insights into electrochemical nitrogen reduction reaction on vanadium nitride nanoparticles. J Am Chem Soc 140:13387–13391
16. Zhao Z, Long Y, Luo S, Luo Y, Chen M, Ma J (2021) Metal-free C_3N_4 with plentiful nitrogen vacancy and increased specific surface area for electrocatalytic nitrogen reduction. J Energy Chem 60:546–555
17. Yu X, Han P, Wei Z, Huang L, Gu Z, Peng S, Ma J, Zheng G (2018) Boron-doped graphene for electrocatalytic N_2 reduction. Joule 2:1610–1622
18. Wang Y, Zhang C, Li X, Gao T, Wang X-B (2021) Metal-free carbon-based nanomaterials for electrochemical nitrogen and carbon dioxide reductions. Mater Res Bull 140:111294–111308
19. Qiu W, Xie X-Y, Qiu J, Fang W-H, Liang R, Ren X, Ji X, Cui G, Asiri AM, Cui G, Tang B, Sun X (2018) High-performance artificial nitrogen fixation at ambient conditions using a metal-free electrocatalyst. Nat Commun 9:3485–3492
20. Zhang L, Ding L-X, Chen G-F, Yang X, Wang H (2019) Ammonia synthesis under ambient conditions: selective electroreduction of dinitrogen to ammonia on black phosphorus nanosheets. Angew Chem Int Ed 58:2612–2616
21. Guo Y, Cheng Y, Li Q, Chu K (2021) $FeTe_2$ as an earth-abundant metal telluride catalyst for electrocatalytic nitrogen fixation. J Energy Chem 56:259–263
22. Yang X, Sun S, Meng L, Li K, Mukherjee S, Chen X, Lv J, Liang S, Zang H-Y, Yan L-K, Wu G (2021) Molecular single iron site catalysts for electrochemical nitrogen fixation under ambient conditions. Appl Catal B: Environ 285:119794–119802
23. Liu P-Y, Shi K, Chen W-Z, Gao R, Liu Z-L, Hao H, Wang Y-Q (2021) Enhanced electrocatalytic nitrogen reduction reaction performance by interfacial engineering of MOF-based sulfides $FeNi_2S_4$/NiS hetero-interface. Appl Catal B: Environ 287:119956–119964
24. Li Y, Li J, Huang J, Chen J, Kong Y, Yang B, Li Z, Lei L, Chai G, Wen Z, Dai L, Hou Y (2021) Boosting electroreduction kinetics of nitrogen to ammonia via tuning electron distribution of single-atomic iron sites. Angew Chem Int Ed 60:9078–9085
25. Liu W, Han L, Wang H-T, Zhao X, Boscoboinik JA, Liu X, Pao C-W, Sun J, Zhuo L, Luo J, Ren J, Pong W-F, Xin H (2020) FeMo sub-nanoclusters/single atoms for neutral ammonia electrosynthesis. Nano Energy 77:105078–105085
26. Wang M, Liu S, Qian T, Liu J, Zhou J, Ji H, Xiong J, Zhong J, Yan C (2019) Over 56.55% faradaic efficiency of ambient ammonia synthesis enabled by positively shifting the reaction potential. Nat Commun 10:341–348
27. Sahoo SK, Heske J, Antonietti M, Qin Q, Oschatz M, Kühne TD (2020) Electrochemical N_2 reduction to ammonia using single Au/Fe atoms supported on nitrogen-doped porous carbon. ACS Appl Energy Mater 3:10061–10069
28. Wang Z, Zheng K, Liu S, Dai Z, Xu Y, Li X, Wang H, Wang L (2019) Electrocatalytic nitrogen reduction to ammonia by Fe_2O_3 nanorod array on carbon cloth. ACS Sustain Chem Eng 7:11754–11759
29. Zhang D, Liu Y, Mao B, Li H, Jiang T, Zhang D, Dong W, Shi W (2021) Double-phase heterostructure within Fe-doped $Cu_{2-x}S$ quantum dots with boosted electrocatalytic nitrogen reduction. ACS Sustain Chem Eng 9:2844–2853
30. Li XF, Li QK, Cheng J, Liu L, Yan Q, Wu Y, Zhang X-H, Wang Z-Y, Qiu Q, Luo Y (2016) Conversion of dinitrogen to ammonia by FeN_3–embedded graphene. J Am Chem Soc 138:8706–8709
31. Han B, Meng H, Li F, Zhao J (2020) Fe_3 cluster anchored on the C_2N monolayer for efficient electrochemical nitrogen fixation. Catalysts 10:974–982
32. Ma Z, Xiao C, Cui Z, Du W, Li Q, Sa R, Sun C (2021) Defective Fe_3GeTe_2 monolayer as a promising electrocatalyst for spontaneous nitrogen reduction reaction. J Mater Chem A 9:6945–6954
33. Lv X-W, Liu X-L, Suo Y-J, Liu Y-P, Yuan Z-Y (2021) Identifying the dominant role of pyridinic-N – Mo bonding in synergistic electrocatalysis for ambient nitrogen reduction. ACS Nano 15:12109–12118
34. Yang Z, Yuan C-Z, Xu A-W (2018) Rationally designed Fe-tetrapyridophenazine complex: a promising precursor to single-atom Fe catalyst for efficient oxygen reduction reaction in high-power Zn-air cells. Nanoscale 10:16145–16152
35. Zhang Z, Yao K, Cong L, Yu Z, Qu L, Huang W (2020) Facile synthesis of a Ru-dispersed N-doped carbon framework

catalyst for electrochemical nitrogen reduction. Catal Sci Technol 10:1336–1342
36. Zhao Y, Li F, Li W, Li Y, Liu C, Zhao Z, Shan Y, Ji Y, Sun L (2021) Identification of M-NH_2-NH_2 intermediate and rate determing step for nitrogen reduction with bioinspired sulfur-bonded FeW catalyst. Angew Chem Int Ed 60:20331–20341
37. Watt GW, Chrisp JD (1952) A spectrophotometric method for the determination of hydrazine. Anal Chem 24:2006–2008
38. Li L, Tang C, Xia B, Jin H, Zheng Y, Qiao S-Z (2019) Two-dimensional mosaic bismuth nanosheets for highly selective ambient electrocatalytic nitrogen reduction. ACS Catal 9:2902–2908
39. Mukherjee S, Cullen DA, Karakalos S, Liu K, Zhang H, Zhao S, Xu H, More KL, Wang G, Wu G (2018) Metal-organic framework-derived nitrogen-doped highly disordered carbon for electrochemical ammonia synthesis using N_2 and H_2O in alkaline electrolytes. Nano Energy 48:217–226
40. Zhao D, Sun K, Cheong W-C, Zheng L, Zhang C, Liu S, Cao X, Wu K, Pan Y, Zhuang Z, Hu B, Wang D, Peng Q, Chen C, Li Y (2020) Synergistically interactive pyridinic-N-MoP sites: identified active centers for enhanced hydrogen evolution in alkaline solution. Angew Chem 132:9067–9075
41. Xia L, Fu W, Zhuang P, Cao Y, Chee MOL, Dong P, Ye M, Shen J (2020) Engineering abundant edge sites of bismuth nanosheets toward superior ambient electrocatalytic nitrogen reduction via topotactic transformation. ACS Sustain Chem Eng 8:2735–2741
42. Alper K, Tekin K, Karagöz S, Ragauskas AJ (2020) Sustainable energy and fuels from biomass: a review focusing on hydrothermal biomass processing. Sustain Energ Fuels 4:4390–4414

Authors and Affiliations

Ying Wang[1] · Hui Luo[1] · Chaoxu Ye[1] · Yanjun Shi[1] · Zhidong Chen[1] · Wenchang Wang[1] · Jianyu Cao[1] · Juan Xu[1]

[1] School of Petrochemical Engineering, Jiangsu Key Laboratory of Advanced Catalytic Materials and Technology, Analysis and Testing Center, Changzhou University, 213164 Changzhou, China